Investigations on the Application of Various Surface Treatments for Trailing Edge Noise Reduction on a Flat Plate

Felix Gstrein*, Bin Zang† and Mahdi Azarpeyvand‡
Faculty of Engineering, University of Bristol, United Kingdom, BS8 1TR

In the present study, a range of different surface treatments is considered for the attenuation of flat plate trailing edge noise through reducing the power spectral density of the unsteady surface pressure fluctuations near the trailing edge. This approach is inspired by the recent studies on finlets, which have proven the trailing edge noise reduction capability of these treatments. To investigate the development of the boundary layer turbulence, measurements of the unsteady surface pressure along the center line and the span of the flat plate are presented. Particular focus is set on the formation and development of turbulence structures in front of and within the treated area. Far-field noise measurement results suggest that the conventional finlets are the most suitable surface treatment to efficiently reduce the trailing edge noise. However, in terms of reducing the unsteady pressure loading on the surface, other configurations produce comparable effects, nevertheless they increase the far-field noise level. The beamforming maps for discrete frequencies suggest that additional noise likely originates from the treatments themselves. Investigations of the static and unsteady surface pressure fields reveal further possible mechanisms related to the overall noise increase. The outcomes of this study thus inform about surface treatment design features important for effective far-field noise reduction.

I. Nomenclature

C_p	=	pressure coefficient
$C_{p,\,\mathrm{rms}}$	=	root-mean-square of the fluctuations of the pressure coefficient
f_c	=	center frequency (Hz)
L	=	length of the conventional finlet treatments (mm)
p_0	=	reference pressure (µPa)
p'_{rms}	=	root-mean-square of pressure fluctuations (Pa)
Re	=	Reynolds number
R_{pp}	=	non-dimensional pressure auto-correlation coefficient
s	=	spacing between conventional finlet wall-structures (mm)
U_∞	=	free-stream velocity ($\mathrm{m\,s^{-1}}$)
x, y, z	=	set-up coordinate system (mm)
x_F, y_F	=	(finlet-) treatment coordinate system (mm)
Λ_z	=	spanwise turbulence correlation length (mm)
τ	=	time lag (s)
ϕ_{pp}	=	unsteady surface pressure power spectral density ($\mathrm{dB\,Hz^{-1}}$)

II. Introduction

The noise emission from airframes or wind energy plants due to their interaction with unsteady flow has become a subject of increasing research interest. One reason for this is the similar noise level of airfame and modern aircraft engines [1, 2]. Furthermore, the increasing demand for a higher proportion of sustainable energy in increasingly strained supply systems [3, 4] requests for more numerous wind energy plants generating noise pollution. A substantial

*PhD Researcher, Mechanical Engineering, felix.gstrein@bristol.ac.uk.
†Lecturer, Aerospace Engineering, nick.zang@bristol.ac.uk.
‡Professor of Aerodynamics and Aeroacoustics, m.azarpeyvand@bristol.ac.uk.

proportion of the noise scattered when airfoils move through a medium is caused by the interaction of the trailing edge with convected turbulence generated on the airfoil surface and is thus called self- or trailing edge noise [5, 6]. The prediction of self-noise for any flow-immersed object with a sharp trailing edge using Amiet's theory [7] is accomplished considering the power spectral density (PSD) of the unsteady surface pressure fluctuations and the spanwise length-scale of turbulence structures at the trailing edge. Thus, when aiming to reduce and control trailing edge noise, efforts are often made to decrease the intensity of surface pressure fluctuations with different active and passive techniques. However, the effects associated with a manipulation of the boundary layer characteristics are hardly predictable. As a consequence, concepts aiming for a reduction of the surface pressure fluctuations on a flow-immersed object often come along with unwanted effects such as additional noise sources and have to be further developed.

Different trailing edge noise reduction techniques can generally be classified as active and passive flow control strategies. With additional energy input, active flow control techniques have been applied to manipulate the boundary layer flow resulting in broadband frequency reduction of trailing edge noise in the form of boundary layer injection [8, 9] or suction [10, 11]. Passive flow control strategies make use of flow-guiding objects or modifications to airfoils or flat plates to reduce the turbulence energy content or minimize areas of flow interaction where noise is scattered into the far-field. Successful implementations include trailing edge serrations [12–14], brushes [15], porous materials [16–18] and surface treatments applied flush with or upstream of the trailing edge [19–24]. The passive flow control strategies were mostly derived from the noise attenuating features of silently flying owl species, where treatments resembling the downy hairs on the surface of an owl feather seem to be the most promising technique for reducing trailing edge noise above 2000 Hz [25].

Conducting experiments with a wide range of different surface treatments on a flat surface at different flow speeds, Clark et al. [19] tried to reproduce the effects of the downy hairs on owl feathers on aerodynamic noise reduction, indicated in the study of Lilley [25]. Using their own photographic study, they reconstructed features of owl feathers in form of hemispheres, vertical needles and sandpaper covered with fabrics. They observed a reduction of the far-field noise of about 5 dB at high velocities (60 m s^{-1}) and frequencies (> 10 000 Hz) and a considerable decrease of surface pressure fluctuations of about 30 dB at frequencies around 2000 Hz and 20 m s^{-1}, for the scenarios where the rough surfaces were covered with fabrics. Moreover, fabrics with fibers oriented perpendicular to the direction of the flow were found to produce self-noise. Trying to establish a treatment suitable for the application on airfoils, Clark et al. [20] later introduced thin wall-structures with a tapered front part oriented in streamwise direction with a certain spanwise distance from each other. Applying these treatments, termed "finlets", flush with the trailing edge of a DU96-W180 airfoil, they achieved up to 10 dB broadband trailing edge noise reduction. Afshari et al. [21] studied finlet treatments mounted upstream of the trailing edge of a flat plate and associated the observed reduction of surface pressure fluctuations with dissipation effects due to friction on the increased wetted surface from the finlets. They also identified a shear layer forming on top of the treatments, causing undesirable flow separation effects in the finlet wake if the distance between the wall structures falls below a certain threshold. By adding a "third dimension", i.e. integrating staggered finlet rows to the conventional finlet treatments, Afshari et al. [22] suppressed the flow separation in the wake of the finlets and observed an increased capacity to reduce trailing edge noise compared to the conventional finlets. In their numerical study, Bodling and Sharma [23] found that lifted turbulence may contribute to the reduction of trailing edge noise when finlet treatments are applied flush with the trailing edge of a NACA 0012 airfoil. The two different noise reduction mechanisms described by Afshari et al. [21] and Bodling and Sharma [23] suggest that the application of finlets leads to different scenarios in terms of trailing edge noise reduction on a flat plate and an airfoil. The physical changes to the boundary layer within the treated area of a flat plate fitted with finlet treatments upstream of the trailing edge were experimentally investigated and discussed by Gstrein et al. [24]. They found that a large part of the surface pressure fluctuation reduction process takes place in the wake of the finlets upstream of the trailing edge. Furthermore, in addition to conventional finlet treatments, they considered a modified finlet treatment with rectangular wall-structures, which led to a level of surface pressure PSD reduction similar to that for the configuration treated with conventional finlets.

The present study investigates various surface treatments applied on a flat plate in an attempt to achieve trailing edge noise reduction. In doing so, the approaches of previous work are used to design modified treatments that are promising toward a reduction of surface pressure fluctuations near the trailing edge. Some treatments have already been examined in other works [20, 22, 24] whereas others have not been considered for noise reduction strategies. The goal is to provide near-field data particularly from within the treated area and associate them with the results for the far-field sound pressure level (SPL). The experimental set-up and measurement techniques are explained in Section III. Results are given in Section IV. Concluding remarks are given in Section V.

III. Experimental Set-up

The experimental approach toward the measurement of aerodynamic and acoustic far- and near-field characteristics of a flat plate with various attached surface treatments is detailed in this section. To obtain sufficient and reliable data, a large flat plate was manufactured and equipped with a number of pressure sensors. The experiments were performed in the aeroacoustic facility at the University of Bristol, which is described in the following, together with the sensors and calibration procedures. Subsequently, the flat plate and the installation in the test section are explained. The designs of the surface treatments are discussed at the end of the section.

A. Facility and Data Acquisition

The aeroacoustic facility at the University of Bristol is an open-jet test section connected to a temperature-controlled closed-circuit wind tunnel. The test section is located in an acoustic chamber which is anechoic above 160 Hz. For the present experiments, a nozzle of 500 mm width and 775 mm height was attached to the wind tunnel, which allows for uniform flow speeds in the range of $10\,\mathrm{m\,s^{-1}}$ to $40\,\mathrm{m\,s^{-1}}$. For the presented results, the free-stream velocity, U_∞, was set to $15\,\mathrm{m\,s^{-1}}$, such that the length-based Reynolds number was $Re \approx 990\,000$. A complete description of the facility and its characteristics is provided in [26].

To record the sound pressure fluctuations in the far-field, a beamforming array was placed above the flat plate such that the center of the array was located directly above the trailing edge of the flat plate with a vertical distance of 1387.5 mm. The beamforming array is a circular Aluminium plate about 850 mm in diameter, which was equipped with 64 Panasonic WM-61 A microphones arranged along 9 spiral arms and in the center of the plate. Both, the design of the plate and the arrangement of microphones are explained in detail by Mayer et al. [27]. For the configuration used, the beamforming results were determined to be reliable between 550 Hz and 3550 Hz, where the uncertainty of the microphones was found to be 1.5 dB for a confidence interval of 95 % [28]. To identify the main source of noise emission, a delay-and-sum approach was applied using the Acoular software introduced by Sarradj and Herold [29]. For one-third octave bands within the valid frequency range, the root-mean-square of the sound pressure fluctuations, p'_{rms}, was determined and the sound pressure level calculated as $\mathrm{SPL} = 20\log_{10}\left(p'_{\mathrm{rms}}/p_0\right)$, where the reference pressure was $p_0 = 20\,\mu\mathrm{Pa}$. Pressure spectra were calculated using a Hanning window and with 2^{12} samples per fast Fourier transform block with 50 % overlap. The presented SPL spectra for the trailing edge noise of the treated and untreated configurations of the flat plate are composed of the SPL for different center frequencies of the frequency bands, averaged over the source area at the trailing edge.

The unsteady surface pressure fluctuations were measured with 45 Knowles FG-23329-P07 pressure transducers mounted beneath 0.4 mm diameter pinholes to avoid pressure attenuation effects by reducing the sensing area [30]. The transducers were arranged in the streamwise direction along the mid span as well as in spanwise direction at several streamwise locations, in order to fully capture the flow characteristics. Prior to and in between of the measurements, the pressure transducers in the flat plate and microphones in the beamforming array were calibrated against a G.R.A.S. 40PL reference microphone, which had been calibrated beforehand using a G.R.A.S. 42AA pistonphone. This calibration procedure has been applied in previous works [8, 10, 17, 24]. To obtain the results for the unsteady surface pressure fluctuations, data was sampled with a frequency of 2^{15} Hz for a duration of 70 s. The surface pressure fluctuation PSD, ϕ_{pp}, was then determined applying Welch's method and a Hamming window with a size of 2^{12} samples and 50 % overlap to get the interim result p'^2_{rms}, which was subsequently transformed to $\phi_{pp} = 10\log_{10}\left(p'^2_{\mathrm{rms}}/p_0^2\right)$. Static pressure data for the calculation of the pressure coefficient, C_p, were gathered from 58 pressure taps fixed to the flat plate similar to the unsteady pressure transducers, connected to a Chell μDAQ-32DTC Smart Pressure Scanner with polyurethane tubing of about 1 m length. During the experiments, the static pressure data was sampled for 60 s with a frequency of 1000 Hz.

B. Flat Plate and Instrumentation

Figure 1 shows a schematic of the experimental set-up for the present investigations. The flat plate has a total length of 1000 mm and is slightly wider than the nozzle, which is 500 mm wide and has a height of 775 mm. To facilitate the manufacturing process, the flat plate is an assembly of multiple parts. As indicated in Fig. 1, the plate was mounted in the test section such that its flat leading edge was flush with the lower lip line of the nozzle orifice. Two sidewalls were mounted as an extension of the nozzle to ensure a two-dimensional flow all the way from the leading to the trailing edge. The global coordinate system is defined at the center of the trailing edge with x describing the streamwise, y the surface-normal and z the spanwise direction. Close to the transition from the nozzle orifice to the flat plate surface, a

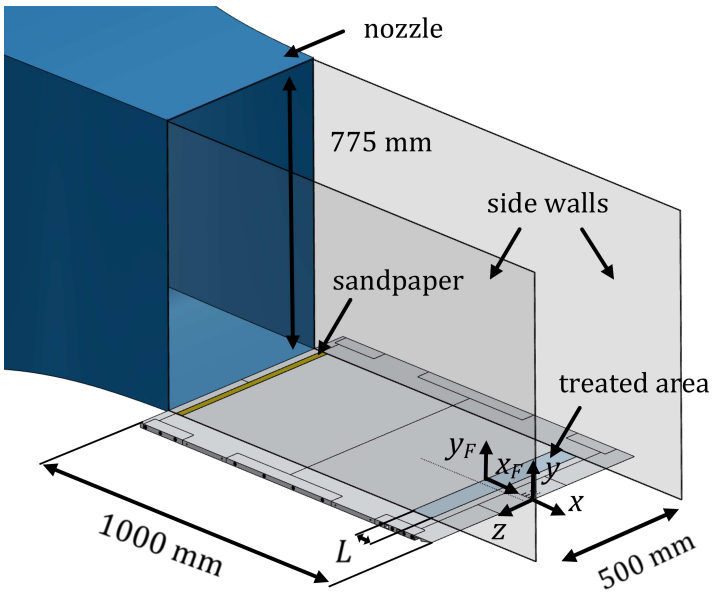

Fig. 1 Schematic of the experimental set-up with nozzle, flat plate and side walls. The area of treatment application is indicated with transparent blue color.

narrow strip of 80-grit sandpaper was fixed to trip the formation of a turbulent boundary layer. All treatments considered in this study were applied such that the treated area starts at $x/L = -2.54$ and the full span of the flat plate restricted by the side walls was covered. A local coordinate system is defined directly in front of the treated area, where x_F denotes the streamwise and y_F the wall-normal component. As mentioned in the previous section, pressure transducers are arranged along the length of this section and toward the trailing edge as well as along the spanwise direction within and in the wake of the treatments. The rear section is tapered with an angle of 12° to form a sharp trailing edge and thus prevent vortex shedding from bluntness. Further details on the flat plate rig can be found in reference [24].

C. Surface Treatment Designs and Dimensions

The surface treatments applied in this study were mainly inspired by rough surfaces such as those investigated by Clark et al. [19], finlets [20, 21, 24] and "three-dimensional finlets" according to the definition of Afshari et al. [22]. Nano-scale surface treatments resembling shark scales have already been considered for skin friction drag reduction [31, 32]. For the discussion of the results in the next section, the treatments are divided into two different groups. The first group is closely related to and also includes the conventional finlets, which consist of thin wall-structures of a certain profile shape, protruding from the flat plate surface. They are usually aligned parallel to the streamwise direction with a defined spacing to each other. The designs and dimensions common to the treatment group are shown in Fig. 2. These treatments have been previously considered for trailing edge noise reduction on a flat plate [22, 24] and were proven to reduce the surface pressure fluctuation spectra near the trailing edge when applied further upstream. Some near-field characteristics for the conventional finlets and finlets with a rectangular profile shape, shown in Fig. 2a, have already been investigated by Gstrein et al. [24]. Thus, the treatments mainly serve as a reference, however, a few additional results will also be presented, such as trailing edge noise. A detailed description of their design can be found in reference [24]. Finlet treatments with two different finlet lengths, where the length changes every second row, as shown in Fig. 2b, were proposed by Afshari et al. [22] and will be further investigated in this study. The profile of the wall-structures is similar to those described in [24].

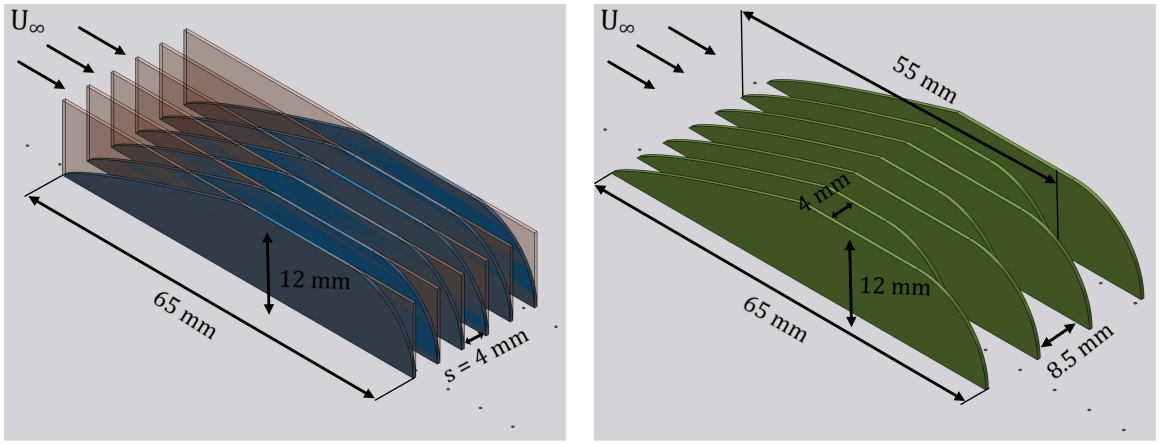

a) b)

Fig. 2 Design and dimensions of different variants of finlets applied on the flat plate surface: a) conventional and rectangular finlets, and b) staggered finlets.

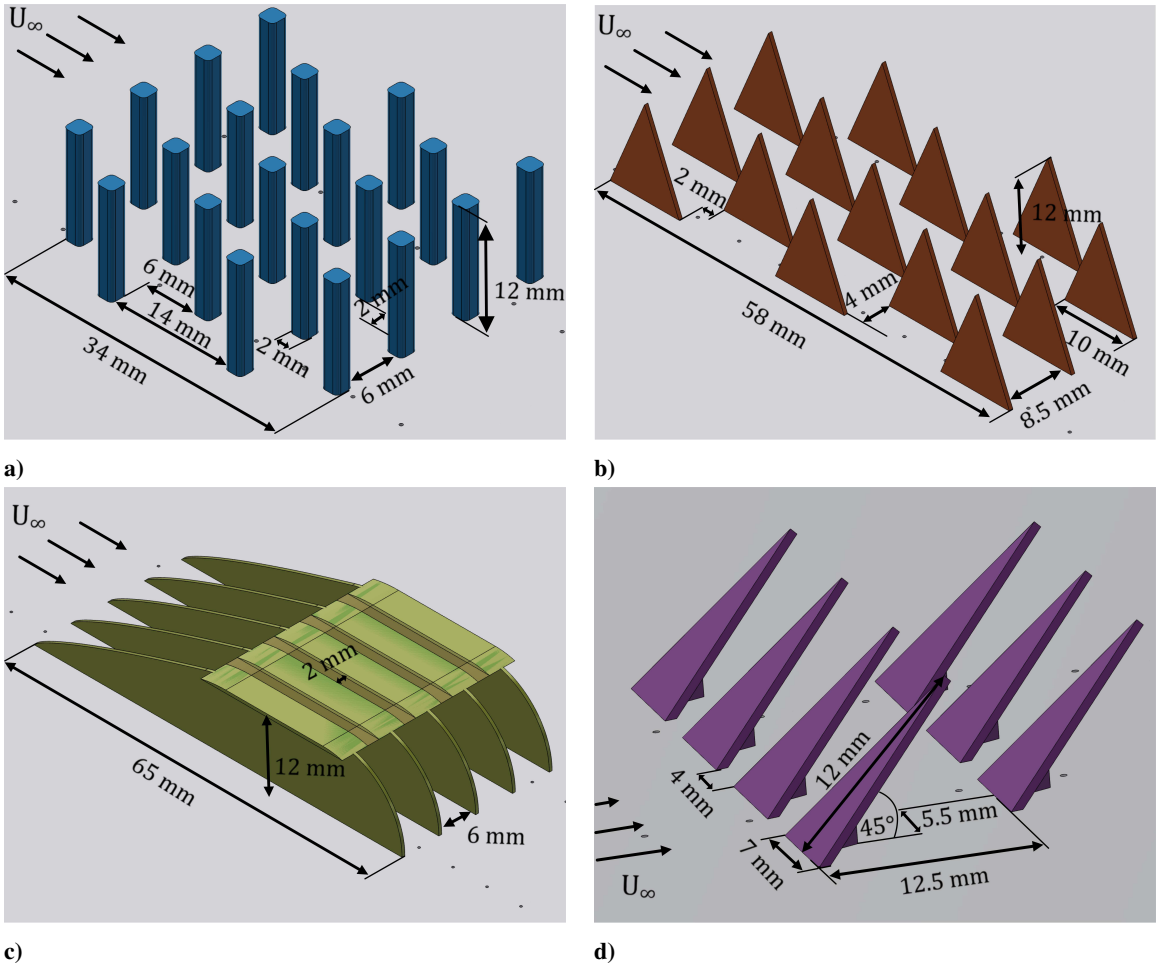

a) b) c) d)

Fig. 3 Design and dimensions of various non-conventional treatments applied on the flat plate surface: a) rods, b) triangles, c) tunnels and T-fronts, and d) scales.

The surface treatments of the second group differ more significantly from the conventional finlet design. They were designed for the purpose of reducing the surface pressure fluctuation spectrum at the trailing edge of the treated flat plate. As illustrated in Fig. 3, the treatment designs are rods protruding from the flat plate surface (Fig. 3a), triangles (Fig. 3b), finlet tunnels or finlets with front profiles resembling a "T" (Fig. 3c) and scales (Fig. 3d). All the treatments have a wall thickness of 0.5 mm and are supported by a 0.3 mm substrate layer base to hold the wall-structures upright in place. In the proximity of sensor locations, the substrates were locally removed to facilitate measurements of the near-field flow characteristics.

IV. Results

In the following, the experimental results for the different variants of the finlets and the non-conventional surface treatments considered are analyzed and compared to those of the conventional finlet treatment. First, the far-field sound pressure level is presented for all the treatments. Then, near-field characteristics and the correlations with and discrepancies to the far-field measurements are discussed.

A. Sound Pressure Level from Trailing Edge Noise

Figure 4 depicts the sound pressure level spectra for the conventional and staggered finlets and those with a rectangular profile shape in comparison with the untreated flat plate, which will be referred to as baseline. It can be observed that the conventional finlets are the most suitable treatment for trailing edge noise reduction. In particular, they decrease the far-field noise emission across the entire frequency range considered with a maximum reduction of approximately 2.6 dB at 1600 Hz. Similarly, the staggered finlets produce an overall noise decrease across the entire frequency range, however, the reduction is clearly less pronounced than for the conventional finlets. According to the beamforming results, the finlets with a rectangular profile shape can significantly reduce the trailing edge noise at low frequencies up to 800 Hz, whereas they cause additional noise at higher frequencies. This result has been expected by Gstrein et al. [24], as they observed tonal peaks in the power spectral density of the unsteady surface pressure.

The far-field SPL results for the group of non-conventional treatments are shown in Fig. 5. As can be seen, all the treatments of this group increase the far-field noise registered by the beamforming array. Since the treatments have been designed to attenuate the unsteady surface pressure fluctuations on the flat plate, it is expected that the increase in far-field SPL is due to a separate mechanism.

To discuss the source of the additional noise generated by the rectangular finlets and the non-conventional treatments, the SPL contours above the flat plate centered at its trailing edge are shown in Fig. 6 at the representative center frequency of f_c = 1000 Hz. Comparing Figs. 6c to 6e with the SPL contour for the baseline shown in Fig. 6a, it can be observed that the main noise source clearly shifts toward the treated area instead of focusing at the trailing edge due to

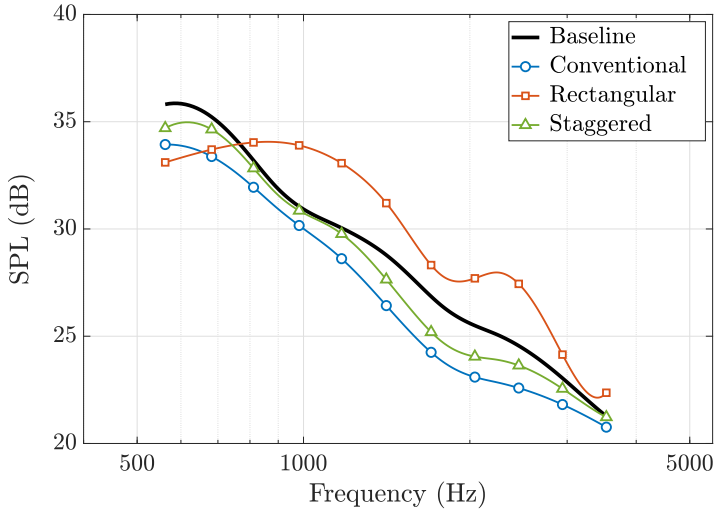

Fig. 4 Far-field SPL for the baseline and the finlet variant configurations.

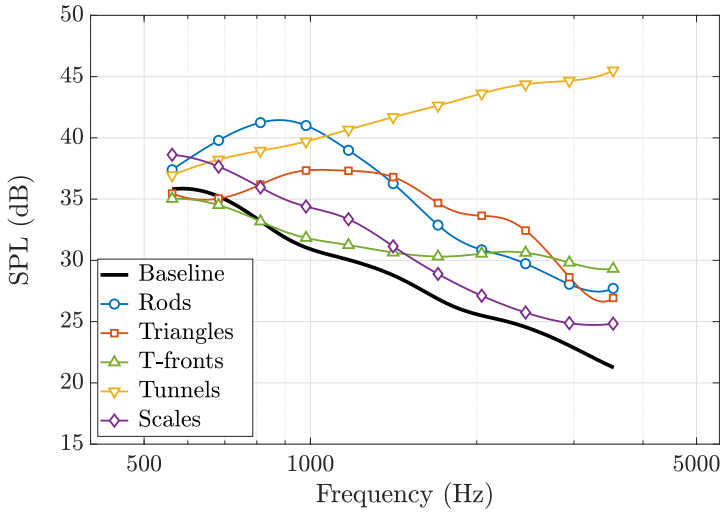

Fig. 5 Far-field SPL for the baseline and the non-conventional treatment configurations.

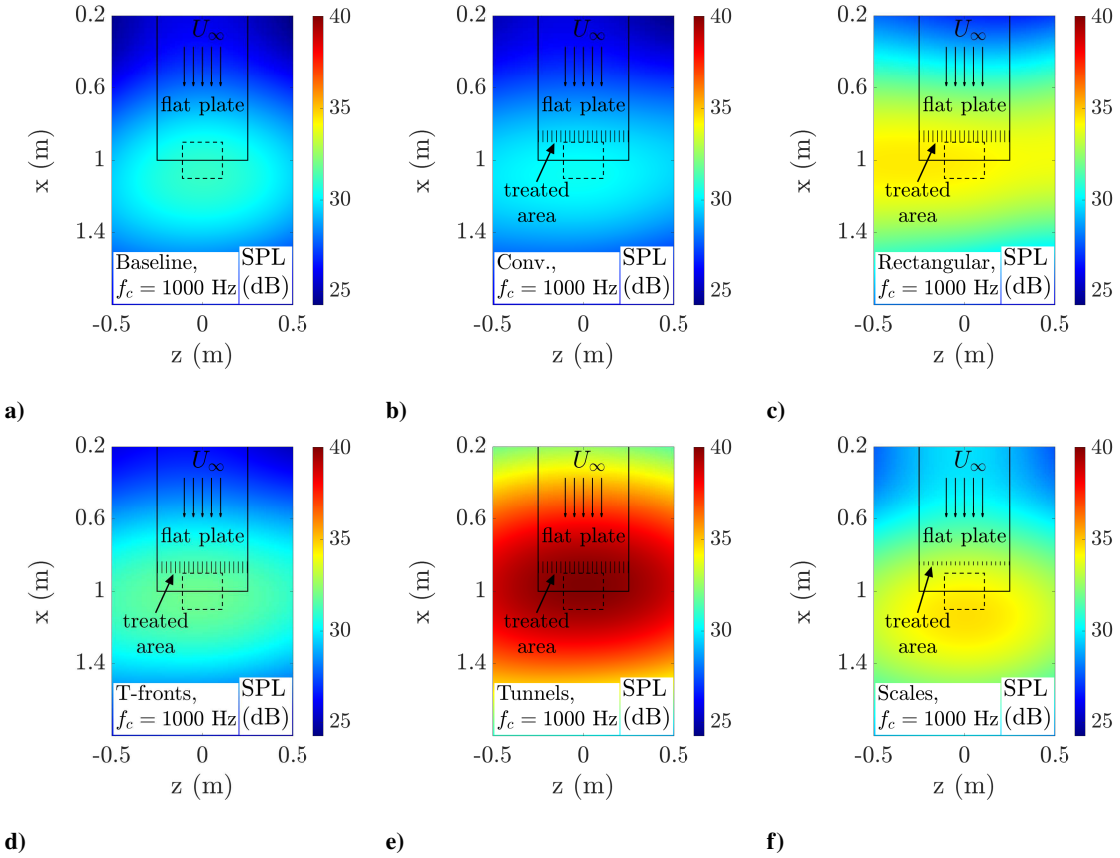

Fig. 6 Beamforming maps at a center frequency of f_c = 1000 Hz: a) Baseline, b) conventional finlet treatment, c) rectangular finlet variant, d) T-fronts, e) tunnels, and f) scales.

the application of the related treatments, i.e. the rectangular finlets, the T-fronts and the tunnels. The characteristics of the SPL contours for the rods and triangles are similar to those for the rectangular finlets and are thus not shown here. In

contrast, the SPL at the trailing edge for the conventional finlet treatment decreases without any detectable additional noise source within the treated area, as shown in Fig. 6b. This suggests that the noise increase from the rectangular finlet and non-conventional treatments except for the scales is not necessarily due to the trailing edge noise, but is radiated directly from the structures they consist of. Thus, the noise is referred to as treatment self-noise in the following. As can be seen from Fig. 6f, in contrast to treatment self-noise, the noise increase due to the application of scales is generated downstream of the trailing edge.

B. Static Pressure Field

Figure 7 shows the static pressure distribution on the flat plate as well as the standard deviation measured at more than 55 different locations for the baseline and the treated configurations. From the development of the pressure coefficient, C_p, along the flat plate treated with finlet variants and non-conventional treatments, shown in Fig. 7a and Fig. 7b, respectively, an adverse pressure gradient can be observed upstream of each of the treatments. Within the treated area, the static pressure drops to recover again rapidly in the treatment wake. The adverse pressure gradient is significantly stronger for the rectangular finlets, the rods and the scales compared to the other treatments, indicating a particularly high resistance to the flow and an unsteady flow transition into the treated area. This is also reflected by the root-mean-square of the pressure coefficient, $C_{p,\,\mathrm{rms}}$, shown in Fig. 7c and Fig. 7d for the finlet variants and the non-conventional treatments, respectively. At the more or less straight leading edges of the rectangular finlets, the rods and the scales, $C_{p,\,\mathrm{rms}}$ and thus the standard deviation of the pressure coefficient are notably higher than at the tapered leading edges of the other treatment types. The static pressure development through the treated area and the quick recovery in the wake of the finlets with steady transitions into and out of the treated area show that the flow smoothly adapts to the wall-structures, where the favorable pressure gradient within the treated area suggests that the bulk flow

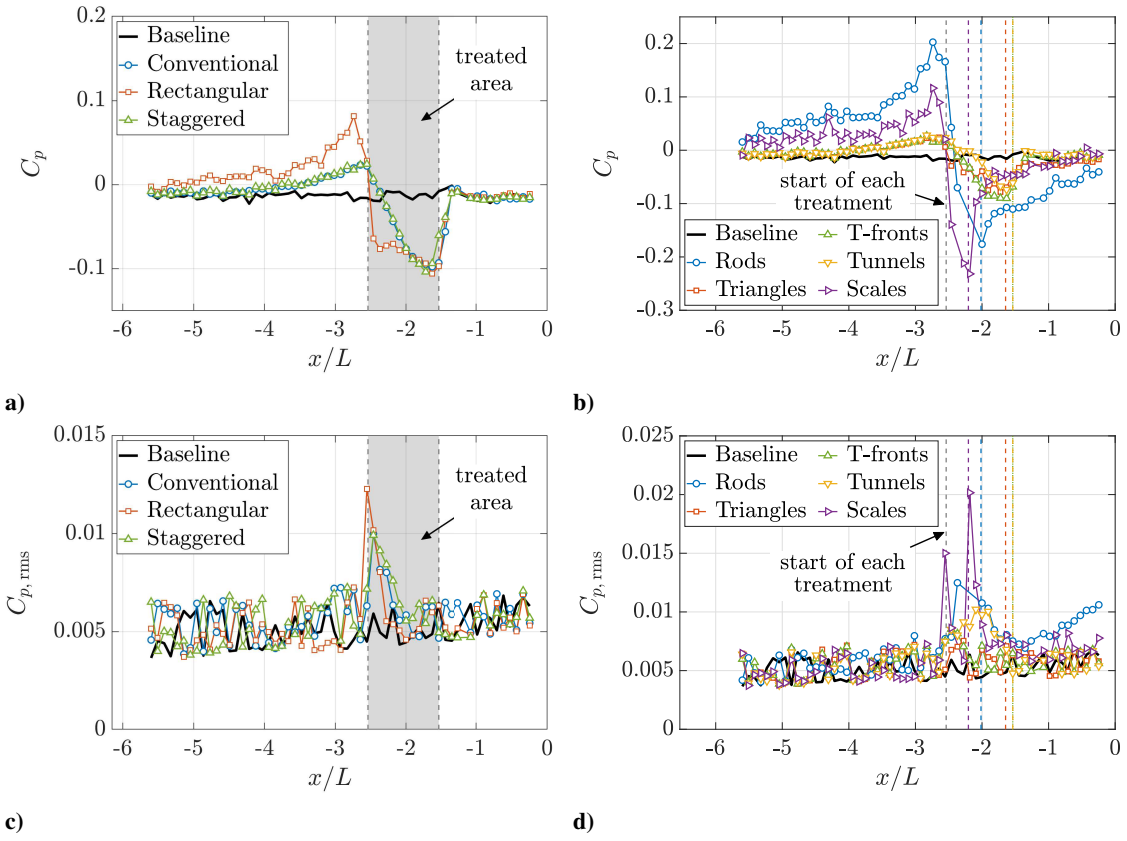

Fig. 7 Pressure coefficient, C_p, and its root-mean-square, $C_{p,\,\mathrm{rms}}$, along the flat plate center line: a) C_p for the finlet variants, b) C_p for the non-conventional treatments, c) $C_{p,\,\mathrm{rms}}$ for the finlet variants, and d) $C_{p,\,\mathrm{rms}}$ for the non-conventional treatments.

has a slight tendency to follow the shape of the finlet profile in a 'softer' way (i.e. the streamlines change from straight- to finlet-shaped).

C. Unsteady Surface Pressure

Figure 8 shows the development of the unsteady surface pressure power spectral density, ϕ_{pp}, from immediately upstream of the area treated with the different variants of finlets to the trailing edge. As can be observed from Fig. 8a, the surface pressure PSD slightly increases immediately upstream of the conventional and the staggered finlets at frequencies below 300 Hz, whereas the fluctuation PSD at higher frequencies is attenuated. The finlets with a rectangular profile shape on the other hand show an increased surface pressure PSD across the entire frequency range, in particular at frequencies lower than 2000 Hz. At higher frequencies, tonal peaks can be observed, similar to the results observed by Gstrein et al. [24]. From Figs. 8b and 8c, it can be seen that the low-frequency part of the spectrum (i.e. the spectrum at frequencies lower than 2000 Hz) decreases again within the rectangular finlets and at the same time the unsteady surface pressure PSD at frequencies above 1000 Hz decreases within the conventional and the staggered finlets, further reducing the pressure fluctuation intensity compared to the baseline. The results for the finlets with a rectangular profile shape again show tonal peaks and exceed those for the baseline at frequencies above 7000 Hz. Immediately downstream of the treated area, all the finlet variants tested show a hump in the unsteady surface pressure PSD between 1000 Hz and 2000 Hz exceeding the results for the baseline, after which the PSD decreases again, as shown in Fig. 8d. A significant reduction of the PSD is observed in the wake of the finlets, developing further toward the trailing edge, which can be seen from Figs. 8e and 8f. The results show that all finlet variants decrease the unsteady surface pressure loading at the trailing edge (see Fig. 8f), where the largest reduction across the frequency range between 60 Hz and 10 000 Hz is attained by the rectangular finlet treatment.

The unsteady surface pressure PSD results for the second group of treatments considered are shown in Fig. 9. Similar to the finlet variants discussed previously, the treatments of this group all produce an increase of low-frequency unsteady surface pressure fluctuation PSD below 1000 Hz, as can be seen from Fig. 9a. At higher frequencies, almost all of the treatments consistently reduce the PSD. The result for the triangles shows several tonal peaks, which is assumed to be the consequence of movements of the flexible wall-structures protruding from the flat plate and thus the treatment sub-layer. Figure 9b depicts the unsteady surface pressure PSD results further downstream. Since the non-conventional treatments have different lengths, as indicated in Fig. 3, the location is within the wake of the scales and the rear section of the rods, whereas for the rest of the treatments it is still within the treated area. Both, the rods and scales show a significantly increased PSD across the entire frequency range considered, compared to the baseline. In contrast, the PSD levels for the other treatments remain low and comparable to the baseline. The data for the triangles, tunnels and T-fronts are characterized by several tonal peaks, occurring at frequencies higher than 3000 Hz. Figure 9d reflects a location outside the treated area for all of the treatments. It can be observed that, following the trend for the rods and the scales at the according location immediately downstream of the respective treated area shown in Fig. 9b, the result for the T-fronts at this transducer position is about 15 dB higher than that for the baseline across the entire frequency range. This behavior is not reflected by the triangles or the tunnels.

Moving further toward the trailing edge, as shown in Figs. 9e and 9f, the PSD decreases for all treatments at frequencies higher than 1000 Hz to significantly fall below the result for the baseline in their wake. Moreover, for all treatments, except for the rods and the scales, the PSD at frequencies below 1000 Hz between the end of the treated area and the flat plate trailing edge does not significantly surpass the results for the baseline in the considered frequency range. This observation suggests that the reason for the far-field noise increase due to the application of rods and scales can in fact be associated with trailing edge noise, generated due to the interaction of the sharp trailing edge with the turbulence related to the increased surface pressure fluctuations between 60 Hz and 1000 Hz.

According to Amiet's theory [7], alongside the unsteady surface pressure PSD, the spanwise length scale of the turbulence, Λ_z, at the trailing edge is a crucial factor for trailing edge noise emission. Thus, Λ_z, determined in the wake of the finlet variants and the non-conventional treatments and normalized by the spacing between the conventional finlet treatments, s, as indicated in Fig. 2a, is presented in Fig. 10. These results have been obtained integrating the coherence (defined as in [6]) between sequential microphones along the span at $x/L = -0.246$ over their separation distance. Figure 10a shows that the spanwise correlation length in the frequency range between 60 Hz and 600 Hz increases significantly for the finlet variants, where the increase is more or less equal for each of the variants. Hence, considering that the conventional finlet treatments overall reduce the trailing edge noise, the results for ϕ_{pp} and Λ_z for the rectangular finlet treatment at the trailing edge suggest that this treatment in comparison with the conventional finlet treatment effects a reduction of the trailing edge noise in a similar manner and extent. However, the beamforming

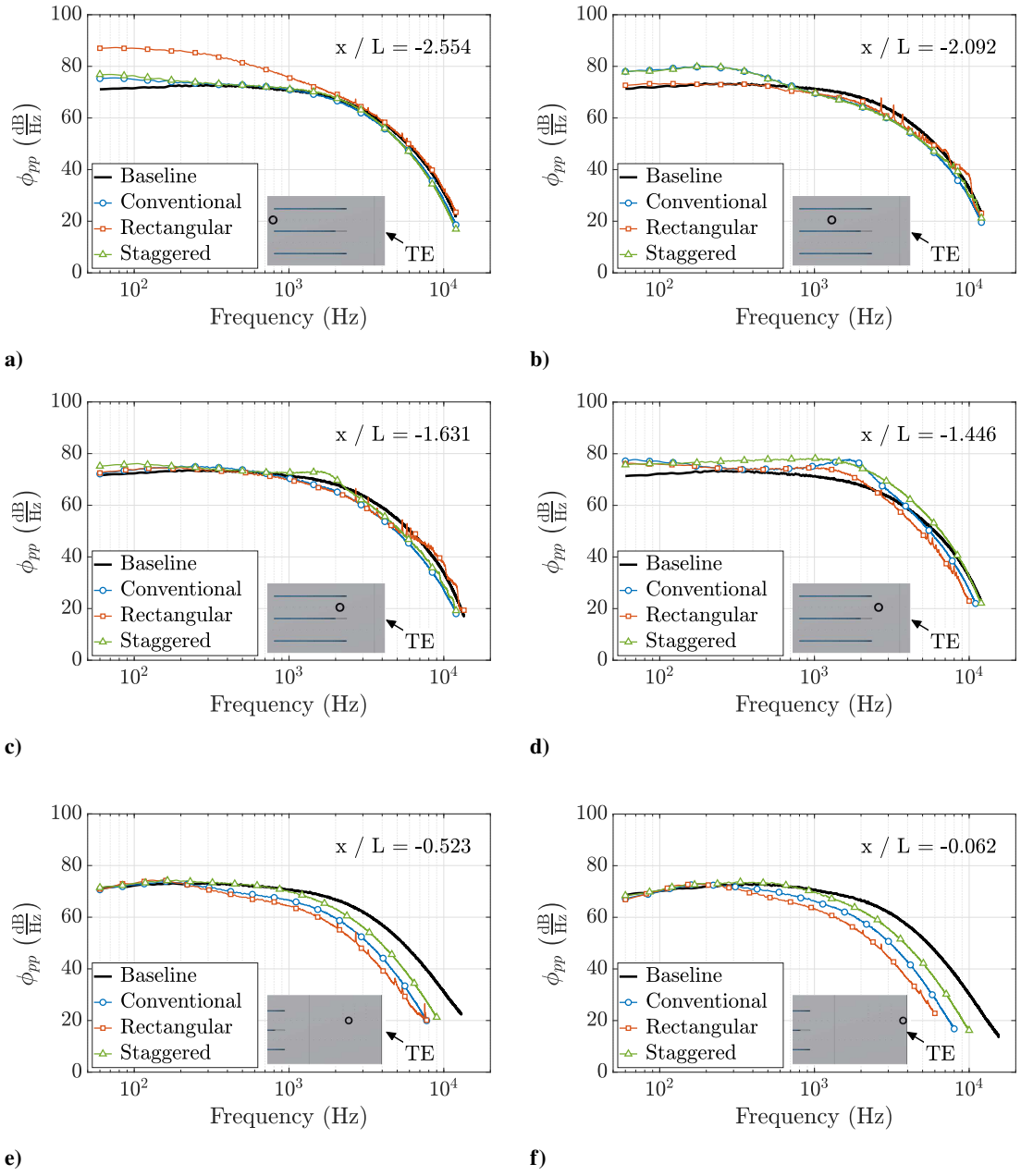

Fig. 8 Unsteady surface pressure PSD for the baseline and the finlet variant configurations: a) $x/L = -2.554$, b) $x/L = -2.092$, c) $x/L = -1.631$, d) $x/L = -1.446$, e) $x/L = -0.523$, and f) $x/L = -0.062$.

contour shown in Fig. 6c and the unsteady surface pressure PSD immediately upstream of the treatment shown in Fig. 8a indicate that the treatment directly emits noise to the far-field. The increase in ϕ_{pp} upstream of the rectangular finlets points to a formation of turbulence structures within a fluctuation frequency range between 60 Hz and 2000 Hz in front of the finlets. Due to the unsteady transition of the flow into the treated area, the turbulence is likely to interact with the straight leading edges of the rectangular finlets, which then produce finlet self-noise. Interestingly, the rectangular shape of the finlets seems to be beneficial for the reduction of the unsteady surface pressure fluctuation PSD in the treatment wake, as observed from Figs. 8d to 8f. This can be explained with the larger wetted area and thus higher surface friction effects that are introduced when compared with the conventional finlets [21]. Also, the unsteady transition from the

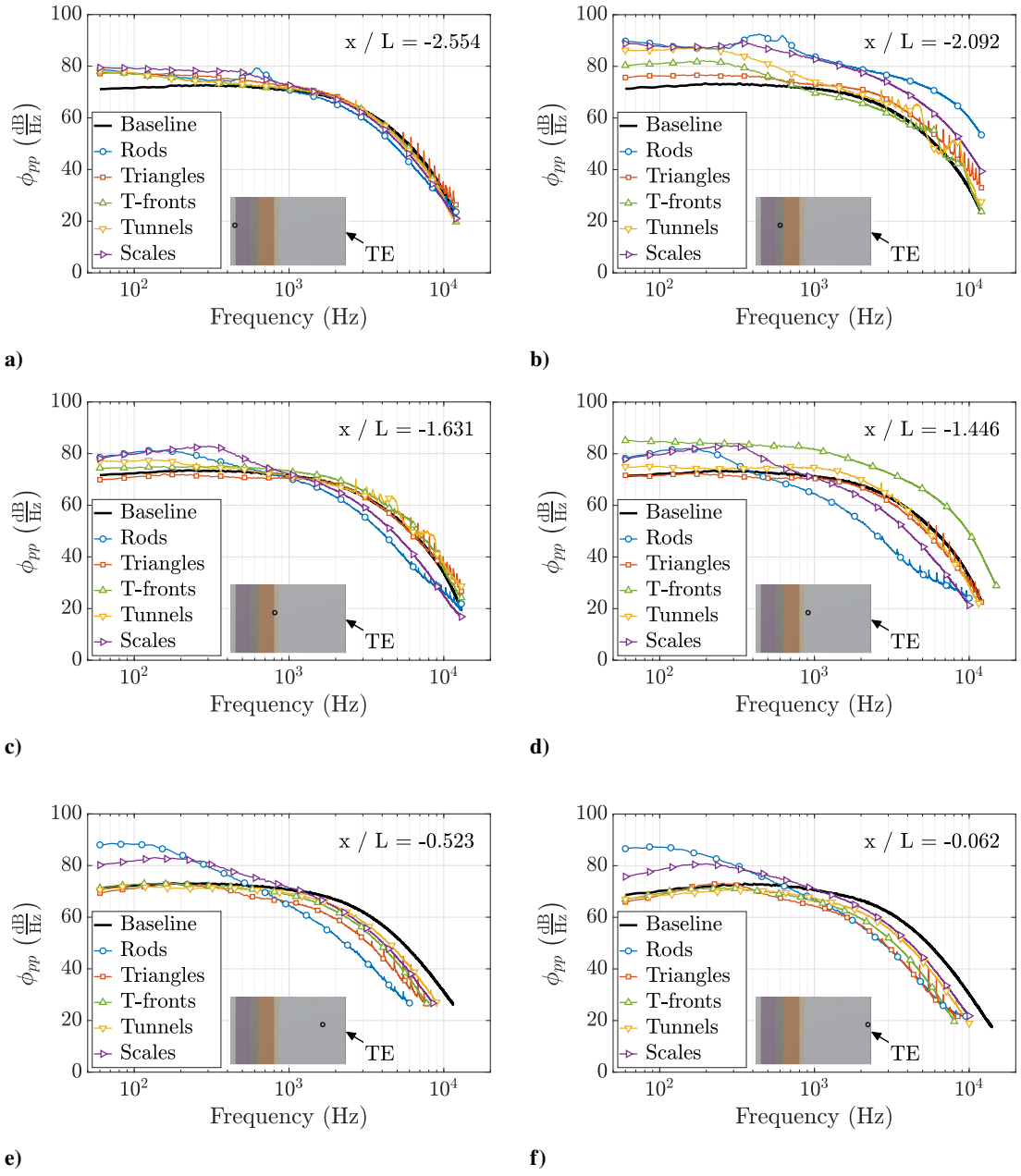

Fig. 9 Unsteady surface pressure PSD for the baseline and the non-conventional treatment configurations with the extent of the application area on the flat plate for each treatment indicated with its assigned color: a) $x/L = -2.554$, b) $x/L = -2.092$, c) $x/L = -1.631$, d) $x/L = -1.446$, e) $x/L = -0.523$, and f) $x/L = -0.062$.

treated area into the treatment wake might have some beneficial effects on the reduction of ϕ_{pp} that can be associated with the mixing of a shear layer building on top of the finlets and the flow channeled through the space between the wall-structures.

Similar to the rectangular finlets, most of the non-conventional treatments increase the spanwise correlation length in their wakes, where the latter remains comparable to the result for the conventional finlets. Thus, it is expected that they are also effective in reducing the trailing edge noise and the additional noise is due to finlet self-noise. However, this scenario is not accurate for the triangles, since the increase in Λ_z at mid frequencies between 200 Hz and 500 Hz for

this treatment is much larger than for all other treatments. Thus, according to Amiet [7], one reason for the overall noise increase at frequencies below 1000 Hz due to the application of triangles can likely be associated with the significantly increased spanwise correlation length of the turbulence structures in the wake of the triangles. Furthermore, the spanwise correlation length in the wake of the tunnels is clearly decreased compared to all other treatments considered, which is probably due to the prevention of an interaction between the channeled flow and the shear layer on top of the treatment because of the closed cover above the wall-structures.

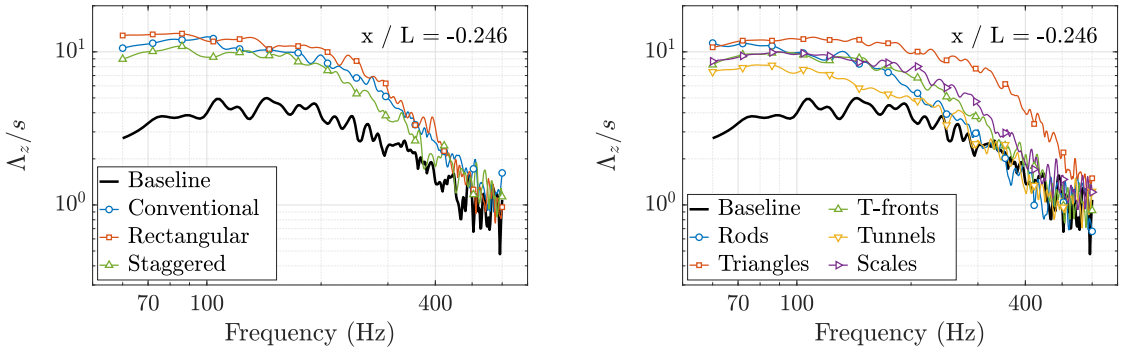

Fig. 10 Spanwise correlation length of the turbulence structures downstream of the treated area at $x/L = -0.246$: a) Finlet variants, and b) non-conventional treatments.

Figure 11 shows the results for the non-dimensional auto-correlation functions in the time domain, R_{pp}, for the baseline and the finlet variants, which are suitable for a closer examination on the nature of turbulence structures forming within the treated area. From Fig. 11a, it can be seen that immediately upstream of the rectangular finlets, which are characterized by a rather unsteady transition into the treated area, the pressure auto-correlation peak widens significantly. Both, a rather low rate of decay at small time lags τ ($\tau U_\infty/L < 0.02$) and an increasing width with growing τ, suggest that highly coherent structures are forming at the leading edges of the rectangular finlets. On the other hand, the correlation peaks for the treatments with a tapered leading edge remain largely comparable to the baseline result, widening only at low auto-correlation values. Thus, they also effect the formation of coherent structures to some extent, which are slightly larger in size (and thus show a low-frequency increase in the PSD). Further downstream within the finlets (Fig. 11b), the peak width collapses for the rectangular finlets, although remaining notably wider than the baseline result below correlation values of $R_{pp} \approx 0.25$. In contrast, the peaks for the staggered and conventional finlet treatments widen, showing a negative maximum at $\tau U_\infty/L = \pm 0.39$. Since these treatment types have tapered leading edges, this observation suggests that the coherent structures exist mainly in the vicinity of the finlet leading edges that interact with the boundary layer flow.

Toward the end of the wall-structures the finlet variants exhibit an oscillating behavior of the pressure auto-correlation function, as shown in Figs. 11c and 11d. The oscillation sets in earlier for the staggered finlet treatments, since every second wall-structure is slightly shorter and thus ends further upstream. This phenomenon points to a periodic pattern immediately downstream of a finlet trailing edge and likely reflects small recirculation areas where the oscillations are more frequent and larger ones for low-frequent oscillations, as for example downstream of the rectangular finlet treatment. It was observed previously [21, 22] that shear layers form on top of finlet treatments, and recirculation effects are likely to set in when the shear layer separates from the finlet ridges to lower toward and reattach with the flat plate surface.

Downstream of the treated area and near the trailing edge (Figs. 11e and 11f), the pressure auto-correlation peaks for the conventional and the rectangular finlet treatments broaden again, suggesting that the free shear layers forming on top of the finlets mix with the channeled flow to form large-scale coherent structures. The staggered finlets seem to influence the mixing process in a way different to the rectangular finlets. In particular, the correlation of the turbulence in their wake is lower, also leading to a slightly lower spanwise correlation length, whereas the rectangular finlets increase both pressure auto-correlation and spanwise correlation length as compared to the conventional finlets. Because of the high correlation at small time lags in the wake of the finlets, the smallest turbulence fluctuations are attenuated, likely due to merging of turbulence structures and viscous dissipation. This happens at the cost of a formation of larger structures,

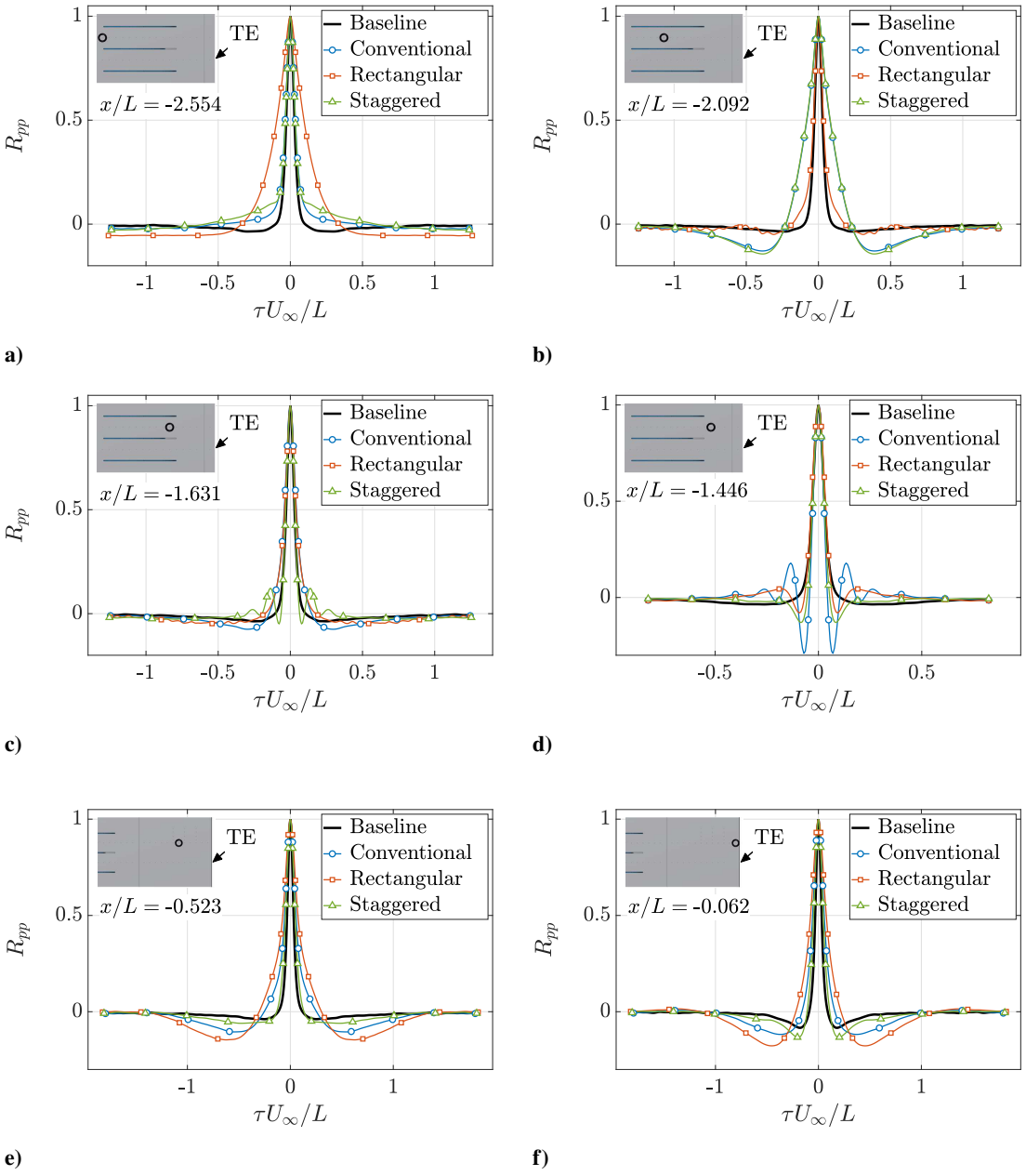

Fig. 11 Non-dimensional pressure auto-correlation coefficients for the baseline and the finlet variant configurations: a) $x/L = -2.554$, b) $x/L = -2.092$, c) $x/L = -1.631$, d) $x/L = -1.446$, e) $x/L = -0.523$, and f) $x/L = -0.062$.

which in turn interact with the flat plate trailing edge. Hence, finlet variants that facilitate this process lead to a reduction of the unsteady surface pressure PSD at high frequencies, but are more prone to the generation of finlet self-noise or low-frequency trailing edge noise.

Figure 12 shows the unsteady surface pressure auto-correlation results for the non-conventional treatments. Note that the treatments are not equally long, such that the distinct locations shown reflect different stages for the flow development through the treated area. The triangles, T-fronts and tunnels overall show trends similar to the finlet variants. However, the rods and scales exhibit more complex flow patterns immediately upstream and within the treated areas. In the wake

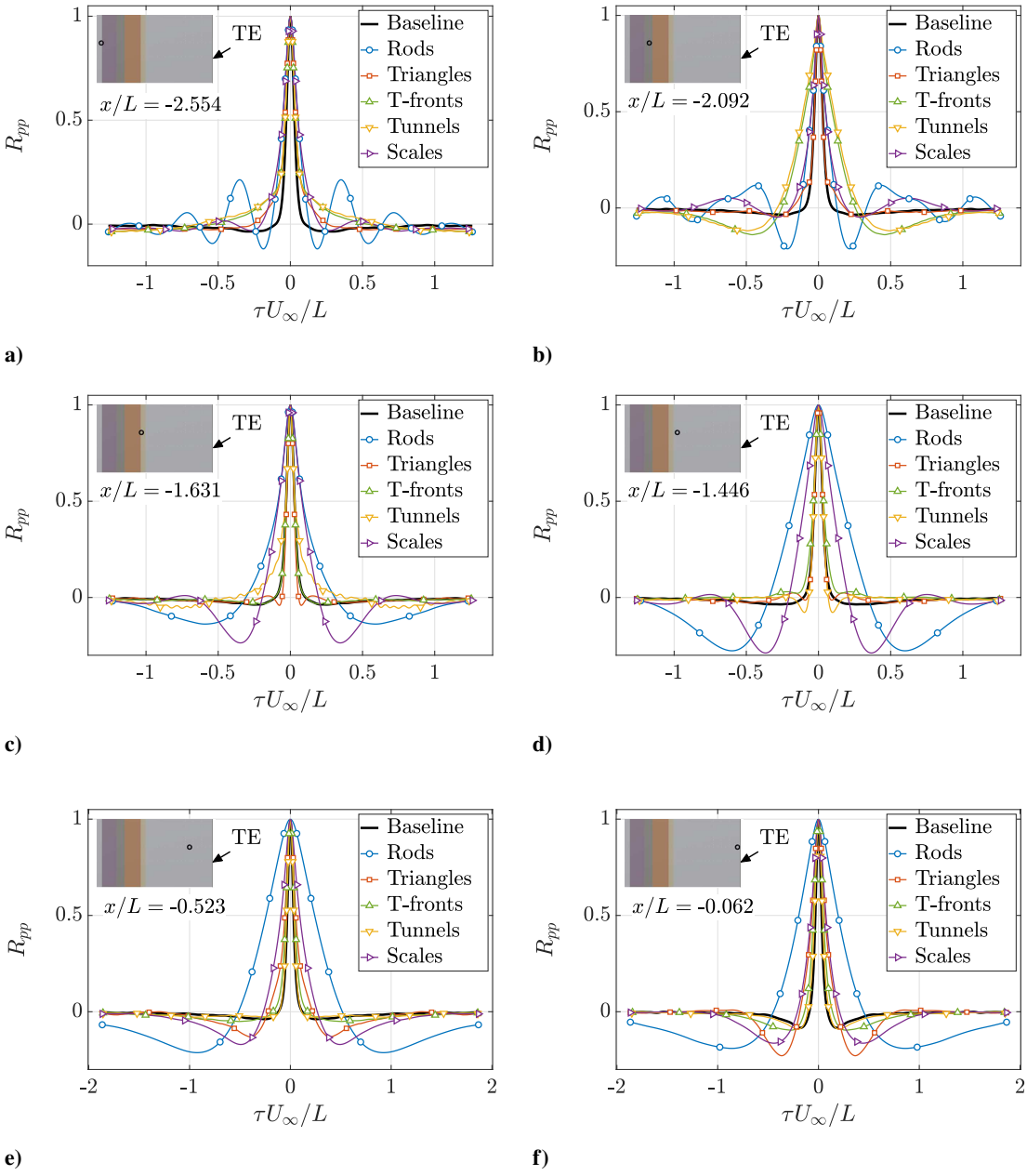

Fig. 12 Non-dimensional pressure auto-correlation coefficients for the baseline and the non-conventional treatment configurations: a) $x/L = -2.554$, b) $x/L = -2.092$, c) $x/L = -1.631$, d) $x/L = -1.446$, e) $x/L = -0.523$, and f) $x/L = -0.062$.

of these treatments, as shown in Figs. 12c to 12f for the scales and Figs. 12d to 12f for the rods, the initial rate of decay is very low, which is the reason for the strong decrease of the surface pressure PSD near the trailing edge. On the other hand, particularly the application of rods leads to a significantly widened auto-correlation peak and thus to large coherent structures that interact with the trailing edge as they are convected past it, which is then likely emitted to the far-field as trailing edge noise at relatively low frequencies.

It should be remarked that so far, the near-field measurements for the T-fronts and the tunnels point to no increase of the trailing edge noise due these treatments. However, the far-field SPL presented in Section IV.A show a severe

increase of the overall noise at frequencies higher than 800 Hz. This contradiction is likely to be related with the canopy or closed roof which these treatments have. It is likely that each horizontal surface creates conditions similar to those on a solid block. This could entail several different noise mechanisms, which can not be identified or even registered by the pressure transducers integrated in the flat plate surface.

V. Conclusions

Different variants of the conventional finlet treatment as well as non-conventional surface treatments differing more significantly from the finlets have been applied on a flat plate and investigated for their capacity for trailing edge noise reduction. It has been found that the conventional finlets are the most suitable surface treatment for trailing edge noise reduction. However, the results for the unsteady surface pressure power spectral density suggest that some of the non-conventional treatments possess the capability to reduce the unsteady surface pressure loading on the flat plate in their wake either across the entire considered spectrum or within a certain frequency range. From the SPL contour maps over the treated flat plate and further investigations of the spanwise turbulence length scale and the development of the unsteady surface pressure fluctuation auto-correlation as well as the static pressure distribution, the reasons for the additional noise due to the application of the non-conventional treatments have been identified. From the outcomes of the present study, the most important features significant for trailing edge noise reduction through treatments applied upstream of the trailing edge can be restricted to three major properties. First, the protruding structures that make up the treatment should channel the flow, i.e. they should guide it through the space between them, where the added surface area within the optimum range of the boundary layer thickness should be large in order to increase the wall-friction effects, which are beneficial for the reduction of high-frequency pressure fluctuations. Second, it is found that the shear layer on top of the treatments, which eventually detaches to mix with the channeled flow, is beneficial for further reduction of the high-frequency pressure fluctuation intensity, likely due to viscous friction effects. Finally, the large surface area and features facilitating a shear-layer are restricted by the needs of creating a smooth transition of the flow into the treated area and avoidance of roofs or canopies introducing further turbulence structures to prevent treatment self-noise.

Acknowledgments

The authors would like to acknowledge the financial support of the EU H2020 ARTEM project under the grant agreement ID 769359. The work of Neil Pearce, who manufactured the flat plate, and Lee Winter, who offered valuable assistance mounting the pressure sensors, is much appreciated.

References

[1] Lilley, G. M., "The prediction of air frame noise and comparison with experiment," *Journal of Sound and Vibration*, Vol. 239, No. 4, 2001, pp. 849–859. doi:10.1006/jsvi.2000.3219.

[2] Lockard, D. P., and Lilley, G. M., "The airframe noise reduction challenge," Tech. mem. tm–2004–213013, NASA, Langley Research Center, Hampton, Virginia, 2004.

[3] Lund, H., "Renewable energy strategies for sustainable development," *Energy*, Vol. 32, No. 6, 2007, pp. 912–919. doi: 10.1016/j.energy.2006.10.017.

[4] Chu, S., and Majumdar, A., "Opportunities and challenges for a sustainable energy future," *Nature*, Vol. 488, No. 7411, 2012, pp. 294–303. doi:10.1038/nature11475.

[5] Brooks, T. F., Pope, D., and Marcolini, M. A., "Airfoil self-noise and prediction," Reference Publication 1218, NASA, Langley Research Center, Hampton, Virginia, 1989.

[6] Glegg, S., and Devenport, W., *Aeroacoustics of Low Mach Number Flows*, Academic Press, 2017.

[7] Amiet, R. K., "Noise due to turbulent flow past a trailing edge," *Journal of Sound and Vibration*, Vol. 47, No. 3, 1976, pp. 387–393. doi:10.1016/0022-460X(76)90948-2.

[8] Szőke, M., Fiscaletti, D., and Azarpeyvand, M., "Effect of inclined transverse jets on trailing-edge noise generation," *Physics of Fluids*, Vol. 30, No. 8, 085110, 2018. doi:10.1063/1.5044380.

[9] Leitch, T. A., Saunders, C. A., and Ng, W. F., "Reduction of unsteady stator-rotor interaction using trailing edge blowing," *Journal of Sound and Vibration*, Vol. 235, No. 2, 2000, pp. 235–245. doi:10.1006/jsvi.2000.2922.

[10] Szőke, M., Fiscaletti, D., and Azarpeyvand, M., "Influence of boundary layer flow suction on trailing edge noise generation," *Journal of Sound and Vibration*, Vol. 475, 11527, 2020. doi:10.1016/j.jsv.2020.115276.

[11] Wolf, A., Lutz, T., Würz, W., Krämer, E., Stalnov, O., and Seifert, A., "Trailing edge noise reduction of wind turbine blades by active flow control," *Wind Energy*, Vol. 18, No. 5, 2015, pp. 909–923. doi:10.1002/we.1737.

[12] Azarpeyvand, M., Gruber, M., and Joseph, P. F., "An analytical investigation of trailing edge noise reduction using novel serrations," *19th AIAA/CEAS Aeroacoustics Conference*, AIAA 2013-2009, Berlin, Germany, 2013, p. 2009. doi: 10.2514/6.2013-2009.

[13] Mayer, Y. D., Lyu, B., Jawahar, H. K., and Azarpeyvand, M., "A semi-analytical noise prediction model for airfoils with serrated trailing edges," *Renewable Energy*, Vol. 143, 2019, pp. 679–691. doi:10.1016/j.renene.2019.04.132.

[14] Chong, T. P., and Vathylakis, A., "On the aeroacoustic and flow structures developed on a flat plate with a serrated sawtooth trailing edge," *Journal of Sound and Vibration*, Vol. 354, 2015, pp. 65–90. doi:10.1016/j.jsv.2015.05.019.

[15] Herr, M., and Dobrzynski, W., "Experimental investigations in low-noise trailing-edge design," *AIAA Journal*, Vol. 43, No. 6, 2005, pp. 1167–1175. doi:10.2514/1.11101.

[16] Geyer, T., Sarradj, E., and Fritzsche, C., "Measurement of the noise generation at the trailing edge of porous airfoils," *Experiments in Fluids*, Vol. 48, No. 2, 2010, pp. 291–308. doi:10.1007/s00348-009-0739-x.

[17] Ali, S. A. S., Azarpeyvand, M., and Da Silva, C. R. I., "Trailing-edge flow and noise control using porous treatments," *Journal of Fluid Mechanics*, Vol. 850, 2018, pp. 83–119. doi:10.1017/jfm.2018.430.

[18] Showkat Ali, S. A., Azarpeyvand, M., Szőke, M., and Ilário Da Silva, C. R., "Boundary layer flow interaction with a permeable wall," *Physics of Fluids*, Vol. 30, No. 8, 085111, 2018. doi:10.1063/1.5043276.

[19] Clark, I. A., Devenport, W., Jaworski, J. W., Daly, C., Peake, N., and Glegg, S., "The noise generating and suppressing characteristics of bio-inspired rough surfaces," *20th AIAA/CEAS Aeroacoustics Conference*, Delft, The Netherlands, 2014, p. 2911. doi:10.2514/6.2014-2911.

[20] Clark, I. A., Alexander, W. N., Devenport, W., Glegg, S., Jaworski, J. W., Daly, C., and Peake, N., "Bioinspired trailing-edge noise control," *AIAA Journal*, Vol. 55, No. 3, 2017, pp. 740–754. doi:10.2514/1.J055243.

[21] Afshari, A., Azarpeyvand, M., Dehghan, A. A., Szöke, M., and Maryami, R., "Trailing-edge flow manipulation using streamwise finlets," *Journal of Fluid Mechanics*, Vol. 870, 2019, pp. 617–650. doi:10.1017/jfm.2019.249.

[22] Afshari, A., Dehghan, A. A., and Azarpeyvand, M., "Novel three-dimensional surface treatments for trailing-edge noise reduction," *AIAA Journal*, Vol. 57, No. 10, 2019, pp. 4527–4535. doi:10.2514/1.J058586.

[23] Bodling, A., and Sharma, A., "Numerical investigation of noise reduction mechanisms in a bio-inspired airfoil," *Journal of Sound and Vibration*, Vol. 453, 2019, pp. 314–327. doi:10.1016/j.jsv.2019.02.004.

[24] Gstrein, F., Zang, B., and Azarpeyvand, M., "A parametric study on the application of finlets for trailing edge noise reduction of a flat plate," *AIAA AVIATION 2020 FORUM*, AIAA 2020-2501, VIRTUAL EVENT, 2020, pp. 1–15. doi:10.2514/6.2020-2501.

[25] Lilley, G. M., "A study of the silent flight of the owl," *4th AIAA/CEAS Aeroacoustics Conference*, Toulouse, France, 1998, p. 2340. doi:10.2514/6.1998-2340.

[26] Mayer, Y. D., Jawahar, H. K., Szőke, M., Ali, S. A. S., and Azarpeyvand, M., "Design and performance of an aeroacoustic wind tunnel facility at the University of Bristol," *Applied Acoustics*, Vol. 155, 2019, pp. 358–370. doi:10.1016/j.apacoust.2019.06.005.

[27] Mayer, Y., Zang, B., and Azarpeyvand, M., "Design of a Kevlar-walled test section with dynamic turntable and aeroacoustic investigation of an oscillating airfoil," *25th AIAA/CEAS Aeroacoustics Conference*, AIAA 2019-2464, Delft, The Netherlands, 2019, p. 2464. doi:10.2514/6.2019-2464.

[28] Celik, A., Bowen, J. L., and Azarpeyvand, M., "Effect of trailing-edge bevel on the aeroacoustics of a flat-plate," *Physics of Fluids*, Vol. 32, No. 10, 2020, p. 105116. doi:10.1063/5.0024248.

[29] Sarradj, E., and Herold, G., "A Python framework for microphone array data processing," *Applied Acoustics*, Vol. 116, 2017, pp. 50–58. doi:10.1016/j.apacoust.2016.09.015.

[30] Gravante, S. P., Naguib, A. M., Wark, C. E., and Nagib, H. M., "Characterization of the pressure fluctuations under a fully developed turbulent boundary layer," *AIAA Journal*, Vol. 36, No. 10, 1998, pp. 1808–1816. doi:10.2514/2.296.

[31] Bhushan, B., "Biomimetics inspired surfaces for drag reduction and oleophobicity/philicity," *Beilstein Journal of Nanotechnology*, Vol. 2, No. 1, 2011, pp. 66–84. doi:10.3762/bjnano.2.9.

[32] Bixler, G. D., and Bhushan, B., "Fluid drag reduction and efficient self-cleaning with rice leaf and butterfly wing bioinspired surfaces," *Nanoscale*, Vol. 5, No. 17, 2013, pp. 7685–7710. doi:10.1039/c3nr01710a.